



Interpretation and topographic compensation of conifer canopy self-shadowing

Van R. Kane^{a,*}, Alan R. Gillespie^b, Robert McGaughey^c, James A. Lutz^a, Kevin Ceder^a, Jerry F. Franklin^a

^a College of Forest Resources, University of Washington, Box 352100, Seattle, WA 98195, USA

^b Earth and Space Sciences, University of Washington, Box 351310, Seattle, WA 98195, USA

^c Pacific Northwest Research Station, USDA Forest Service, University of Washington, Box 352100, Seattle, WA 98195, USA

ARTICLE INFO

Article history:

Received 5 June 2007

Received in revised form 5 June 2008

Accepted 6 June 2008

Keywords:

Topographic correction
Topographic normalization
Topographic compensation
Forest canopies
Canopy complexity
Canopy structure
Canopy self-shadowing
Rumple
Spectral mixture analysis

ABSTRACT

The self-shadowing of conifer canopies results from the size and arrangement of trees within a stand and is a first-order term controlling radiance from forested terrain at common pixel scales of tens of meters. Although self-shadowing is a useful attribute for forest remote-sensing classification, compensation for the topographic effects of self-shadowing has proven problematic. This study used airborne canopy LiDAR measurements of 80 Pacific Northwest, USA conifer stands ranging in development stage from pre-canopy closure to old-growth in order to model canopy self-shadowing for four solar zenith angles (SZA). The shadow data were compared to physical measurements used to characterize forest stands, and were also used to test and improve terrain compensation models for remotely sensed images of forested terrain. Canopy self-shadowing on flat terrain strongly correlates with the canopy's geometric complexity as measured by the rumple index (canopy surface area/ground surface area) ($R^2=0.94-0.87$ depending on SZA), but is less correlated with other stand measurements: 95th percentile canopy height ($R^2=0.68$), mean diameter at breast height (dbh) ($R^2=0.65$), basal area ha^{-1} ($R^2=0.18$), and canopy stem count ha^{-1} ($R^2=0.18$). The results in this paper support interpretation of self-shadowing as a function of canopy complexity, which is an important ecological characteristic in its own right. Modeling of canopy self-shadowing was used to assess the accuracy of the Sun-Canopy-Sensor (SCS) topographic correction, and to develop a new empirical Adaptive Shade Compensation (ASC) topographic compensation model. ASC used measured shadow (as an estimate of canopy complexity) and the SCS term (to describe the illumination geometry) as independent variables in multiple regressions to determine the topographic correction. The ASC model provided more accurate radiance corrections with limited variation in results across the full range of canopy complexities and incidence angles.

© 2008 Elsevier Inc. All rights reserved.

1. Introduction

The ability to use canopy self-shadowing to classify and derive stand parameters in forest remote sensing has long been recognized (e.g., Li and Strahler, 1985). Because stands with trees of different sizes, shapes, and arrangements cast different amounts of shadow, self-shadowing as a fraction of the image correlates with the complexity of the canopy structure. This allows classification based on forest structure using differences in the canopy self-shadowing (Fig. 1a–b). Table 1 summarizes terminology related to shadowing as used in this paper.

Canopy self-shadow is frequently used in spectral mixture analysis (SMA) of moderate-resolution images (e.g., Landsat Thematic Mapper, TM), to analyze canopy structure at sub-pixel scales. SMA estimates sub-pixel fractions of spectrally distinct and physically meaningful endmembers as estimates of the proportion of materials in an image

(Adams and Gillespie, 2006; Adams et al., 1993, 1995; Foody, 2004; Settle and Drake, 1993). In images of forest landscapes, spectral endmembers for green vegetation (GV), non-photosynthetic vegetation (NPV) such as wood, soil, and topographic shading and shadow (spectrally grouped as “Shade”: Adams and Gillespie, 2006) are commonly used. At pixel scales of tens of meters, canopy self-shadowing is the dominant contribution to Shade for conifer forests (e.g., Gillespie et al., 2006).

Adams et al. (1995) used Shade to distinguish between Amazonian forest types based on the self-shadowing differences of dominant tree species. Peddle et al. (1999) found that use of the Shade endmember improved estimation of boreal forest biophysical properties. Lu et al. (2003) used SMA with the Shade endmember for Amazonian forest classification and biomass estimation. Sabol et al. (2002) used the Shade fraction in the Pacific Northwest, USA, to rank stands by structural stage from early canopy closure (20–30 years old) through old-growth (>200 years old). Tottrup et al. (2007) found that increases in the Shade fraction corresponded with greater forest maturity in Southeast Asia.

Although the use of canopy self-shadowing is perhaps best developed with SMA, it is also used with other remote-sensing

* Corresponding author.

E-mail address: vkane@u.washington.edu (V.R. Kane).

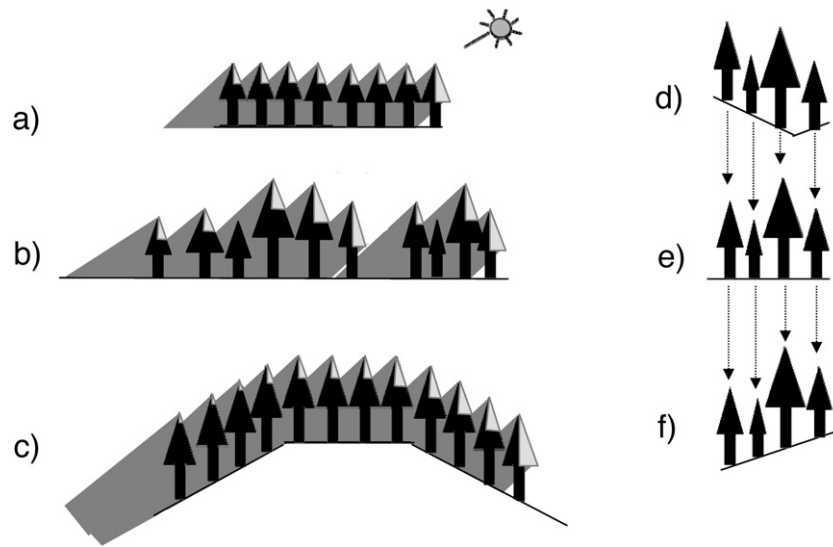


Fig. 1. Effect of canopy complexity and topography on tree shade. Simple forest canopies (a) create less tree shade than complex canopies (b). For any stand within a forest, topography decreases tree shade on sun-facing slopes and increases tree shade on slopes facing away from the sun, changing the area of sunlit canopy (bright canopy areas). Variations in topography can mimic variations in canopy complexity, increasing the difficulty of classifying stand complexity (c). Bright areas on tree figures in 1–c show sunlit canopy area; rest of canopy area would be in shadow. This study uses LiDAR-derived canopy models (d) and adjusts the underlying topography to represent the canopy as it would exist on flat terrain (e). Tree shade is then modeled using the hillshade function of ArcGrid with 183 slope-aspect combinations (f) and 80 canopy surface models.

methodologies. Shadow is an important component of the Tasseled Cap Wetness transformation that has been used to classify forests based on structural stage (Cohen and Spies, 1992). The proportion of area in tree shadow also has been used in high-resolution (<1 m) satellite remote sensing to estimate forest biomass (Leboeuf et al., 2007) and to estimate diameter at breast height (dbh) and crown area (Greenberg et al., 2005).

Correlation of Shade with ground-measured stand characteristics has proven difficult. Many remote-sensing studies use data such as tree species, dbh, and tree stem density from ground-level plot studies to interpret and validate their satellite images (e.g., Song and Woodcock, 2002). Ground-level measurements, however, commonly correlate poorly with the canopy surface as seen in satellite images, making the interpretation of Shade ambiguous. Allometrically derived canopy surfaces may understate the complexity of canopies, underlining the need for more quantitative measures of fine-scale structure. Topographically induced changes in shading and shadowing create additional ambiguity and are major sources of variation in Landsat images (Gu and Gillespie, 1988).

This study directly examines the relationship of canopy structure and self-shadowing. Airborne LiDAR (Light Detection And Ranging) data were used to model the exposed canopy surface of 80 conifer stands in the Pacific Northwest ranging from pre-canopy closure to old-growth. We use the LiDAR data to address two questions essential to forest studies that use tree shade:

- How well do common measures of stand characteristics correlate with innate canopy self-shadowing?
- Can the topographic influence on self-shadowing be removed while preserving the innate, topographically independent Shade differences between closed-canopy conifer stands (i.e., tree shade of horizontal surfaces plus leaf shade)?

In this paper, we first investigate the correlation of canopy shadowing to common measures of stand characteristics. The use of canopy shadowing to analyze forest conditions requires that purely topographic effects on canopy shadowing be accurately corrected. Therefore, we next investigate canopy shadowing and models that relate shadowing to geometric factors of slope and illumination. We then test the leading topographic correction model (SCS) with canopy

shadowing as measured from LiDAR digital elevation models (DEMs). Finally, we substitute an empirical function relating canopy shadowing to geometric factors into radiance correction models for the suppression of topographic effects. We call this the Adaptive Shade Compensation (ASC) model. Because canopy shadowing is a dominant factor controlling canopy radiance (Gu and Gillespie, 1988), shadow-correction models are also radiance correction models that can be used for reducing the effects of topography in images.

1.1. Forests and tree shade

Canopy complexity of conifer forests in the Pacific Northwest generally increases as stands mature (Franklin and Dyrness, 1988; Franklin et al., 2002). At canopy closure, stands are characterized by short trees (relative to their mature heights), high tree densities, and homogeneous canopies (Acker et al., 1998; Franklin et al., 2002; Oliver and Larson, 1996). As stands develop, they have fewer but taller canopy

Table 1
Terminology related to the spectral endmember shade

Term	Definition
Shading	Darkening due to illumination variation controlled by viewing and illumination geometry
Shadow	Dark image object resulting when topographic objects block sunlight
Self-shadowing	Unresolved shadowing due to objects (e.g., trees) within a pixel as opposed to shadowing from resolved shadowing from up-sun objects in other pixels
Shade (capitalized)	Low-amplitude spectrum used as a spectral endmember in spectral mixture analysis and resulting from a combination of shading and unresolved shadows, or from resolved shadows (Adams and Gillespie, 2006)
shade (uncapitalized)	Generic term for shading and shadowing in the landscape and not restricted to the spectral sense of Shade as used in Spectral Mixture Analysis
Hill shade, topographic shade	Darkening due to shading as defined above, by topography and solar illumination angle
Tree shade	Darkening due to canopy self-shadowing generally calculated assuming trees are solid, opaque objects
Leaf shade	Unresolved shadowing within a tree caused by leaves, stems, and other elements comprising the tree
Geometric shade	Darkening due to changes in incidence angle across the surfaces of the individual elements of the tree

trees and heterogeneous, deeply structured canopies. A LiDAR study of Pacific Northwest conifer canopies found that canopy complexity (rugosity) increased with stand age (Ogunjemiyo et al., 2005). Canopy self-shadowing also increased when measured by the SMA Shade endmember as canopies age and develop more complex structures (Roberts et al., 2004; Sabol et al., 2002).

Considerable variation exists within this overall pattern of canopy development. Within the young age class, stand complexity varies at fine scales based on establishment patterns (Winter et al., 2002a) and local disturbances (Lutz and Halpern, 2006) and at coarser scales based on stand-management practices such as the density of re-planting, herbicide application, and mechanical thinning (Smith et al., 1997). Within old-growth age classes, canopy complexity depends on a stand's disturbance history (Bradshaw and Spies, 1992; Franklin and Van Pelt 2004; Franklin et al., 2002; Larson and Franklin, 2006; Winter et al., 2002b; Zenner, 2004). Edaphic, topographic, and climatic factors can introduce additional variation (Poage and Tappeiner, 2005).

This study examines the relationship between common measures of stand structure (e.g., mean dbh) and two sources of spectral Shade. *Tree shade* consists of the visible shadows cast by one tree or branch on another, and is created by the geometric complexity of the canopy (Fig. 1). It does not include any topographic shading, as modeled by cosine and related models that assume smooth, diffuse surfaces. *Topographic shade* in forested terrain is the reduction of scene radiance through changes in the area of tree shade caused by topography and solar zenith angle. Thus tree shade is a function of the shape and spacing of trees, and also terrain. In this paper, stand and canopy complexity refer to the size and arrangement of trees and the geometric complexity of the canopy surface and not to other sources of complexity such as species diversity.

1.2. Previous efforts at forest topographic compensation

Topography changes the radiance measured in remotely sensed images. It is commonly assumed that for smooth terrain, irradiance – and hence radiance – is controlled by the sun-terrain-sensor geometry alone, but in forests shadowing is the dominant source of spatial variance (Gu and Gillespie, 1988).

A number of papers have proposed methods to compensate for topographic variation of radiance of forest scenes (Table 2) (Dymond et al., 2001; Gu and Gillespie, 1988; Soenen et al., 2005, Soenen et al., 2008; Teillet et al., 1982; Vincini and Frazzi, 2003). The radiance cosine correction (Eq. (3)) (Teillet et al., 1982), for example, attempts to compensate for topography by normalizing the sun-terrain-sensor geometry, without consideration of shadowing. Radiance cosine-based corrections assume that the surface is a perfect diffuse reflector. Teillet et al. (1982) also suggested the use of the Minnaert radiance correction (Eq. (4)) (Minnaert, 1941), which empirically modifies the cosine correction through a constant k that is derived through a regression that determines how closely the observed surface behaves as a diffuse Lambertian reflector. The radiance C correction (Eq. (6)) (Teillet et al., 1982) modifies the cosine correction (Eq. (3)) with a C constant that is empirically derived using the relationship between measured illumination and incidence angle to moderate over- and under-correction at extreme pro- and anti-sun slopes. Teillet et al. (1982) found, however, that the Minnaert and C empirical corrections did not improve conifer forest classification accuracy.

Gu and Gillespie (1988) directly addressed the problem of topographic correction of conifer forests and approached the problem by recognizing the dominant role of shadowing. Cosine-based corrections assume that changes in image radiance were caused by changes in the angle between the sun, surface, and sensor. Forests, however, present a special case for topographic correction because trees grow geotropically (upright with respect to Earth's gravity) rather than perpendicular to local slopes. The slopes of the surfaces within a tree canopy that reflect light, therefore, do not change with changes in

Table 2

Nomenclature (a) and equations (b) commonly discussed for topographic correction of radiance for conifer canopies

(a) Nomenclature	
Symbol	Explanation
i	Incidence angle (degrees)
θ	Solar Zenith Angle (degrees)
α	Slope (degrees)
ϕ	Terrain azimuth relative to sun (degrees)
L, L_n	Illumination for uncorrected and corrected topography (units)
k	Minnaert correction constant
e	Exitance angle (degrees)
C	C correction constant
b_0, b_1, b_2	Coefficients for linear regressions
ϵ	Energy falling on a pixel per unit time (W)
E_s	Solar terrestrial irradiance (W m^{-2})
S, S_n	Pixel surface area (m^2) for uncorrected slopes and corrected horizontal slopes, respectively
I, I_n	Average irradiance on canopy surface (W m^{-2}) for corrected and uncorrected slopes, respectively
A, A_n	Sunlit canopy area on a surface within a pixel (m^2) for uncorrected and corrected, and flat slopes respectively. A measured from LiDAR data and hillshade modeling; A_n estimated using topographic correction functions.
$ShA, ShA_n, ShA_{\text{flat}}$	Shadowed canopy area (proportion) for uncorrected, corrected, and flat slopes respectively. ShA and ShA_{flat} measured from LiDAR data and hillshade modeling; ShA_n estimated using topographic compensation functions. Used as estimates of the SMA Shade fraction from tree shade.
(b) Equations	
Notes	Equation
Incidence angle	$\cos i = \cos \theta \cos \alpha + \sin \theta \sin \alpha \cos \phi$ (1)
Cosine correction	$L_n = \frac{L}{\cos i}$ (2)
Modification of cosine correction proposed by Teillet et al. (1982)	$L_n = L \frac{\cos \theta}{\cos i}$ (3)
Minnaert correction (Minnaert, 1941) cosine correction (Eq. (3)) modified with an empirically derived value k	$L_n = L \left[\frac{\cos \theta}{\cos i} \right]^k$ (4)
where k is derived from	$L = L_n (\cos^k i) (\cos^{k-1} e)$ (5)
C correction (Teillet et al., 1982) modifies the cosine correction (Eq. (3)) with a C constant that is empirically derived using the relationship between measured illumination and incidence angle. C term moderates over correction at extreme $\cos i$ values.	$L_n = L \frac{\cos \theta + C}{\cos i + C}$ (6)
where	$L = b_0 + b_1 \cos i$; and $C = \frac{b_0}{b_1}$ (7)
SCS correction (Gu and Gillespie, 1988) corrects radiance by estimating sunlit area as a fraction of total canopy area.	$L_n = L \frac{\cos \alpha \cos \theta}{\cos i}$ (8)
SCS + C correction (Soenen et al., 2005) adds C term calculated through Eq. (7) to SCS correction to moderate over correction at extreme extreme $\cos i$ values.	$L_n = L \frac{\cos \alpha \cos \theta + C}{\cos i + C}$ (9)

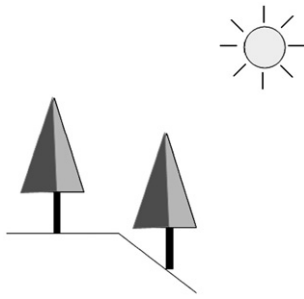
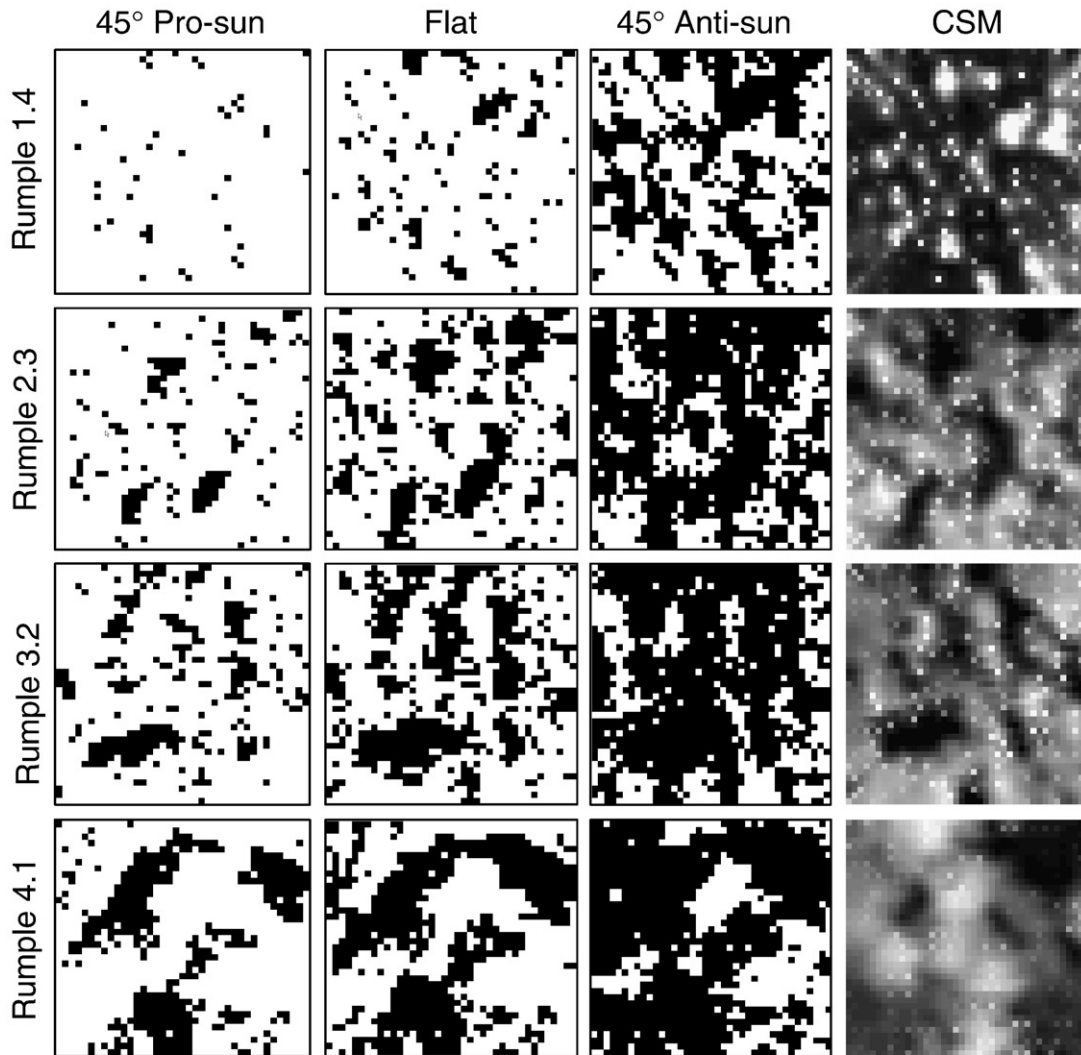


Fig. 2. Radiance from tree canopies is independent of changes in topography. In this illustration, the distance between the two trees and the sun angle prevents shadowing of one tree by another. If the canopy of each tree is the area of one pixel and the pixels are centered on each tree, then the radiance observed from each tree would be identical, even though the underlying surface topography is different.

underlying topography. As a result, the radiance from the illuminated portion of a tree remains constant regardless of the underlying topography (Fig. 2) (Gu and Gillespie, 1988; Soenen et al., 2005).

Gu and Gillespie (1988) observed, however, that topography did change the relative placement of trees with respect to each other and the sun. As a result, the mutual shadowing of trees changes with changes in topography (Figs. 1 c and 3). When shadowing increases on anti-sun slopes, less area of the canopy is sunlit and reflectance measured by the sensor is reduced. As slopes become progressively more pro-sun, the area of shadowed canopy decreases, and radiance measured by the sensor increases. Because the slopes of surface elements such as leaves within the canopy itself do not change with topography, changes in reflectance or radiance with topography are caused by changes in the area of sunlit canopy. Gu and Gillespie (1988) developed their radiance Sun-Canopy



	Shadow Proportion			
Rumple	Pro-sun	Flat	Anti-Sun	CSM range (m)
1.4	0.03	0.10	0.42	0.3 - 16.1
2.3	0.11	0.29	0.67	2.5 - 37.1
3.2	0.19	0.37	0.71	2.1 - 47.7
4.1	0.26	0.44	0.70	1.2 - 77.7

Fig. 3. Changes in area of canopy self-shadowing calculated from canopy surface models (CSMs) derived from LiDAR data for canopy surfaces used in this study. Canopy surfaces are the same as those used for Figs. 4 and 7. Changes in self-shadowed area from different topographies would change both measured radiance and the Shade fraction from spectral unmixing. Solar zenith angle was 33°. Each CSM was 60×60 m.

Table 3
Mathematical derivation of SCS equation (from Gu and Gillespie, 1988)

Notes	Equation
Total solar energy intercepted by a pixel is a function of irradiance, pixel area, and the incidence angle	$\epsilon = E_s S \cos i$ (10)
Total area of the sunlit portion of the canopy can be estimated using the average irradiance of the sunlight canopy	$A = \frac{\epsilon}{I} = E_s S_n \cos i$ (11)
Ratio of the sunlit portion of the canopy on sloped terrain to flat terrain	$\frac{A}{A_n} = \frac{E_s S_n \cos i}{E_s S_n I \cos \theta}$ (12)
Simplification using $I = I_0$ and substituting $S_0 = S \cos(\alpha)$	$\frac{A}{A_n} = \frac{\cos i}{\cos \alpha \cos \theta}$ (13)
Expression in terms of radiance, where radiance is determined by sunlit areas. L_n and A_n have inverse relationships because of Eq. (15)	$\frac{L}{L_n} = \frac{A}{A_n} = \frac{\cos i}{\cos \alpha \cos \theta}$ (14)
Re-arrangement of terms	$L_n = L \frac{\cos \alpha \cos \theta}{\cos i}$ (15)

Unlike traditional topographic correction equations that normalize the geometry of the surface, SCS normalizes the relative area of sunlit versus self-shadowed canopy. Full discussion of the derivation of the SCS equation can be found in Gu and Gillespie (1988). Nomenclature defined in Table 2.

Sensor (SCS) radiance correction (Table 2, Eq. (8)) based on changes of sunlit canopy area rather than attenuated irradiance caused by topographic changes (Table 3, Eq. (13)).

Gu and Gillespie (1988) predicted the sunlit area A_n on a horizontal slope

$$A_n = A \frac{\cos \alpha \cos \theta}{\cos i} \tag{16}$$

as a function of A , the sunlit area on a slope, and the slope α and solar zenith angle, SZA (in the principal plane incidence angle i is the difference between α and SZA).

Because all portions of a canopy are either sunlit or shadowed,

$$S = A_n + ShA_n \tag{17}$$

and

$$ShA_n = S - A_n \text{ (absolute area) or } ShA_n = 1 - A_n \text{ (proportional area)} \tag{18}$$

it is clear that the SCS term

$$\frac{\cos i}{\cos \alpha \cos \theta} \tag{19}$$

is also related to the area of shadow as well as the sunlit area. SCS values decrease as topography slopes away from the sun and increase as topography slopes towards the sun (Fig. 4). This matches the expected behavior of canopy self-shadowing where the sunlit area increases as slopes become progressively more pro-sun.

Gu and Gillespie (1988) acknowledged several limitations of their correction. First, like the radiance cosine correction on which it is based, it over-corrects on anti-sun slopes. Soenen et al. (2005) proposed adding the C term to SCS to reduce this problem (SCS+C correction: Eq. (9)). Second, the SCS model does not take into account any differences in self-shadowing behavior that canopies of different complexity exhibit as slope and aspect changes. Finally, the relationship of canopy complexity and sunlit area may behave differently with different solar zenith angles. (The latter two limitations apply to all the correction methods discussed to this point.) These issues may have contributed to the SCS equation's varying performance when tested by Gu and Gillespie (1988) against forest images.

Summarizing, the SCS model explicitly equates the radiance from a forested slope (L/L_n) to the sunlit area (A/A_n). The sunlit area, and hence the shadowed area, was modeled by a geometric term

(herein the “SCS term”) related to the topographic slope and the solar zenith angle. Gu and Gillespie (1988) expressed concern that the SCS term might not accurately correct sunlit areas because of the variability of conifer canopies. It follows from this reasoning that an improved SCS term that was a function of canopy structure as well as the existing geometric factors might provide improved radiance correction.

Limitations of topographic correction models to deal with canopies of different complexity are a particular concern in the Pacific Northwest. In this region, the height and age of stands permit a range of stand complexities and resulting canopy complexities found in few places of the world (Van Pelt and Nadkarni, 2004; Waring and Franklin, 1979). Preliminary analysis of tree-shade models confirmed that the range of canopy complexities would be a problem for topographic correction. More complex canopies produced lower proportions of sunlit area than less complex canopies for a given incidence angle. In addition, the change in sunlit area for canopies of different complexities was not linear with change in local SZA. These observations suggested that existing topographic correction algorithms would not compensate for the change in self-shadowed area across the range of canopy complexities. A

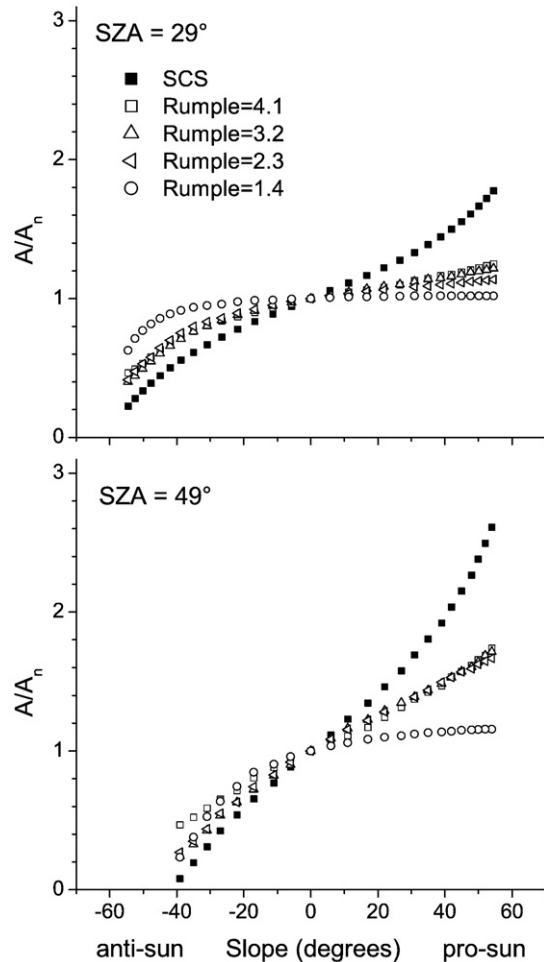


Fig. 4. Relationship of the SCS term (Eq. (19)) to the correct A/A_n correction factor as determined by LiDAR for four plots with different canopy complexities (rumple indices). Higher rumple indices indicate more complex canopies. Correction factors shown for slopes in the principal plane (azimuth relative to the sun of 0° and 180°). The SCS correction factor is fixed for each SZA for a given slope and azimuth, while the A/A_n changes with canopy complexity. Correction factors for simple canopies (rumple <2) follow different curves than correction factors for complex canopies. Therefore, using the SCS geometric correction factor results in different correction accuracies depending on the canopy complexity.

method that adapts to the variable tree-shade behavior of canopies is required.

2. Methods

2.1. Study area and field data

The Cedar River Municipal Watershed lies west of the city of Seattle in the western front of the Cascade mountain range in King County, Washington state, USA (47.4° N, 121.9° W). The Cedar River Watershed has 34,591 ha of forests ranging in elevations from 170 m to 1656 m. The lower part of the watershed lies in the western hemlock (*Tsuga heterophylla*) vegetation zone, the majority the upper watershed in the Pacific silver fir (*Abies amabilis*) zone, and the very highest elevations in the mountain hemlock (*Tsuga mertensiana*) zone (Franklin and Dyrness, 1988). Intensive timber harvests began in the lower elevations in the 1920s, and proceeded into higher elevations until harvesting largely ceased in the 1980s. The majority of the Watershed's forests (84%) are less than 100 years old and established following harvest (Erckmann et al., 2000). Unharvested primary forests over 200 years old with mature and old-growth stand characteristics account for the remaining forested area (16%) (Erckmann et al., 2000). Young forests typically consist of even-aged stands. While structural diversity is typically low in these age classes, variation exists as the result of differences in establishment, site productivity, and disturbance histories. The old-growth stands are remnant patches found primarily in the Pacific silver fir zone. These stands show considerable structural diversity that is a product of differences in age, site productivity, and disturbance histories.

The Cedar River Watershed managers maintain a network of 115 permanent sample plots laid out on an approximate grid throughout the watershed. Of these 115 plots, 80 plots of predominantly coniferous forest were selected for study. (Thirty-five plot sites were eliminated either because of lack of forest cover, deciduous species presence >5% by basal area, LiDAR point densities <0.7 m⁻², or missing forest inventory data.) Stand ages for plots used in this study ranged from 16 years to >300 years (with scattered older trees) and were distributed by age as follows: <49 years: 21 plots; 50–99 years: 34; and >200 years: 25.

Plot data were collected between July 2003 and October 2005. Plot sizes varied from 0.04 to 0.16 ha (0.44–1.8 Landsat pixels), with plot radius chosen to include a sample of a minimum of 25 live trees with dbh >12.7 cm. A handheld Global Positioning

System (GPS) reading was taken at the center of each plot. All trees >12.7 cm dbh were recorded by species, dbh, and crown class with dominant, co-dominant, and intermediate trees extending into the stand canopy and overtopped trees standing entirely beneath the stand canopy.

Each plot was ranked on a stand development scale to help interpret its developmental stage. The Index of Old-Growth (I_{og}) (Acker et al., 1998) compares stands using structural sub-components of mean dbh (cm), standard deviation of dbh (cm), trees ha⁻¹, and count of trees with dbh >100 cm ha⁻¹. Mean values for young and old-growth stands collected by Spies and Franklin (1991) are used to establish the minimum and maximum values for each component:

$$I_{og} = 25 \sum_{j=1}^4 \left[\frac{X_{j,obs} - X_{j,young}}{X_{j,old} - X_{j,young}} \right] \quad (20)$$

where j is each of the four structural sub-components, *obs* is the observed value, *young* is the mean value for young stands from Spies and Franklin (1991), and *old* is the mean value for old-growth stands from Spies and Franklin (1991). Sub-component scores are constrained to be no lower than 0 and no higher than 25. I_{og} scores for plots used in this study ranged from 0 (4 plots) to 100 (3 plots) and were distributed as follows: $I_{og}=0-25$: 20; $I_{og}=26-50$: 17; $I_{og}=51-75$: 28; and $I_{og}=76-100$: 15.

2.2. LiDAR data and analysis

LiDAR data were collected by Spectrum Mapping, LLC using their DATIS II system during leaf-off conditions over the winter of 2002–2003. The scanner used a unidirectional linear pattern with scan angles of $\pm 13.5^\circ$ with a nominal ground footprint of 0.46 m. First return point density for the plots used in this study ranged from 0.70 m⁻² to 1.79 m⁻² (mean 1.00 m⁻²). We used raw LiDAR data with X, Y, Z, and return number values. LiDAR data was processed with a beta version of the Fusion software package derived from release 2.51 (McGaughey and Carson, 2003; McGaughey et al., 2004; USDA Forest Service, 2007).

A ground surface model for the entire Watershed was created from the LiDAR dataset. The Fusion tool set was used to identify ground points in the LiDAR dataset using a 9.14-m moving window. Then a ground surface Digital Terrain Model (DTM) was created from the ground points using the minimum value within a moving 7.62-m window. Areas without ground points were filled by Fusion by interpolation using adjacent values.

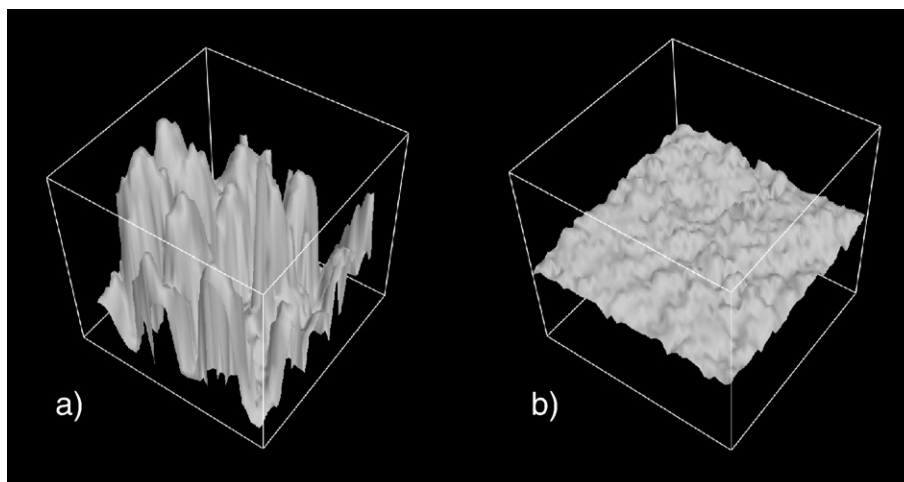


Fig. 5. Examples of canopy surface models created over 60 × 60 m areas from LiDAR data. An old-growth forest patch (a) has a rumple index of 6.2, an index of old-growth (I_{og}) score of 100, and a 95th percentile canopy height of 57 m. A young forest (b) has a rumple index of 1.5, an I_{og} score of 19, and a 95th percentile canopy height of 7.6 m.

Table 4
Solar illumination data used for tree-shade modeling and topographic correction

SZA	29°	33°	39°	49°
Equivalent image date	June 21	July 21	August 20	September 19
Sun elevation	61°	57°	51°	41°
Solar azimuth	138°	139°	146°	155°

Solar zenith angles (SZA) were selected to match parameters for Landsat images of the Cedar River Watershed (Path 46, Row 27 centered at 47° 27' 30"N, 121° 52' 47"W). Illumination parameters calculated with the ENVI 4.0 remote-sensing software.

For each plot, a subset of the LiDAR point cloud for a 60×60-m area centered on each plot's GPS locations was created. The dimensions of the subset were a compromise between including an area large enough to sample the heterogeneity of taller stands (Van Pelt and Nadkarni, 2004; Zenner, 2005) while minimizing the number of study sites with areas that included points from adjacent stands with

different tree sizes. When creating the subsets, the elevation of the ground surface was subtracted from the height of each LiDAR return to produce a point cloud as it would exist on flat terrain (Fig. 1d–f). A canopy surface model (CSM) was created for each study site from the LiDAR subsets (Fig. 5) using a 3×3 smoothing algorithm. The cell size for the CSMs was 1.52 m, which was selected as the smallest cell size that produced realistic canopies.

Five metrics were calculated for each sample site from the LiDAR data:

- Mean point height
- Standard deviation of point heights (also known as the rugosity index, Parker et al., 2004)
- 95th percentile height
- Canopy cover (percentage of first returns >3 m in height divided by total number of first returns)

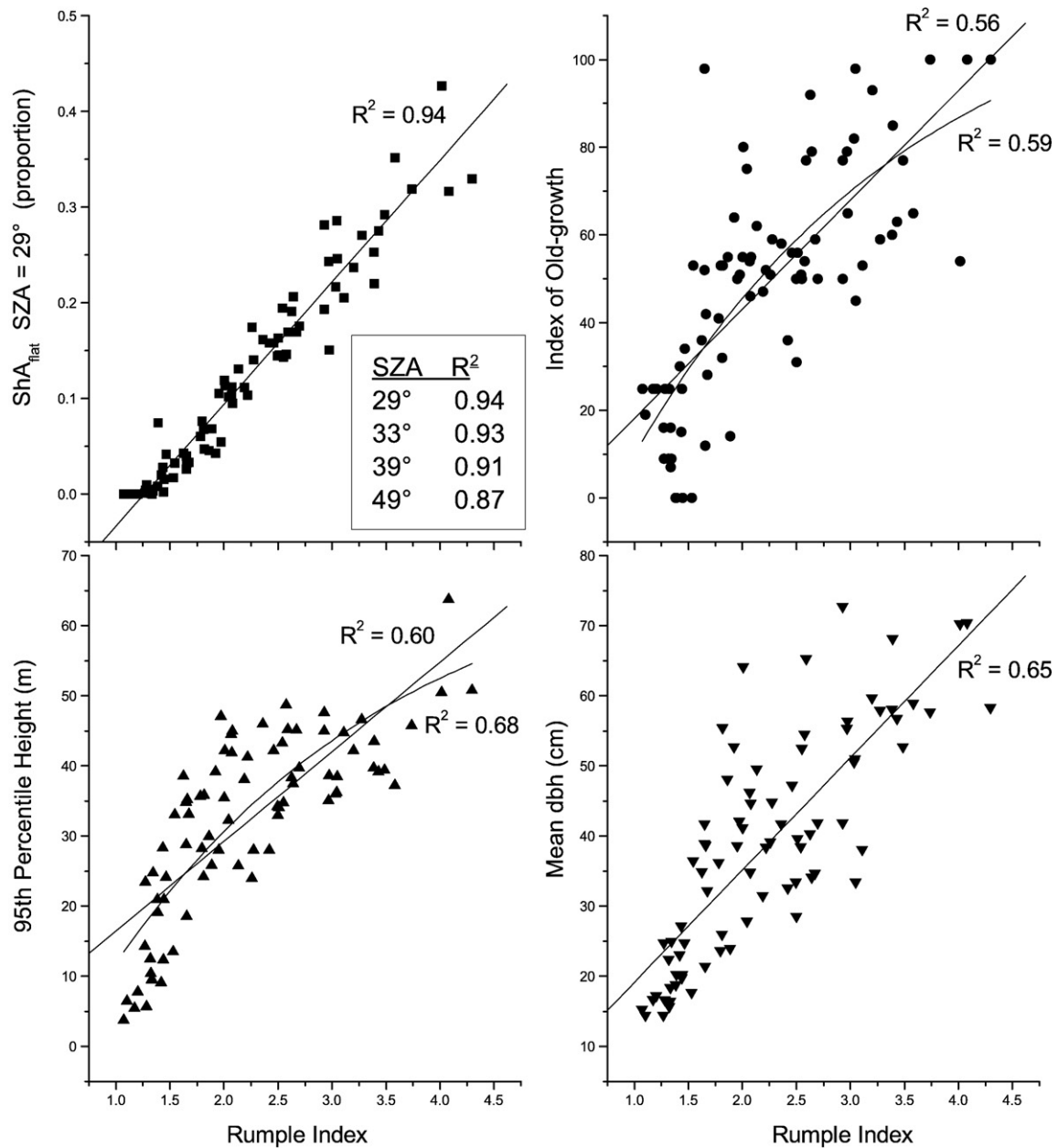


Fig. 6. Relationship of the rumples index to stand characteristics for SZA=29°. The correlation with modeled tree shade on flat terrain was high (a) (values for other SZAs also shown). ShA_{flat} R^2 values for other solar zenith angles of 33°, 39°, and 49° were 0.93, 0.91, and 0.87, respectively. Correlation between the rumples index and stand parameters decreased with increasing rumples index values. Because tree shade on flat terrain was strongly correlated with the rumples index, the ability to extract stand characteristics from measured tree shade decreases with greater stand complexity. All relationships were significant ($P < 0.01$).

Table 5
Coefficients of determination between plot-level stand characteristics and LiDAR data (adjusted R^2)

	Rumple index	Flat shade	I_{og}	P95	Mean dbh	St dev dbh	Basal area
Rumple index ^a							
Flat shade (SZA = 29°) ^a	0.94						
Index of Old-growth (I_{og}) ^b	0.56	0.51					
95th% height (m) (P95) ^a	0.60	0.52	0.53				
Mean dbh ^b	0.65	0.60	0.65	0.67			
Standard deviation dbh ^b	0.54	0.47	0.76	0.48	0.47		
Basal area ^b	0.18	0.16	0.37	0.44	0.43	0.38	
Trees ha ^{-1b}	0.18	0.17	0.32	0.10	0.25	0.09	0.00 ^c

Linear regression relationships are shown (logarithmic regressions with higher R^2 are shown in Fig. 6). All relationships are significant ($P < 0.05$) except as noted.

^a Calculated from LiDAR data using all first returns for each 60×60 m (0.36 ha) sample site.

^b Calculated from plot data (0.04–0.16 ha); since plots were smaller than LiDAR samples used to model tree shade, plot data may not be representative of the entire LiDAR sample area.

^c Not significant.

- Canopy surface area (including ground surface where gaps were present) divided by the ground surface area (“rumple index”: Parker et al., 2004). The rumple index was computed using a site’s canopy surface grid points to create a triangular irregular network of three dimensional points, summing the area of all triangles, and dividing by the ground surface area.

The height and canopy cover metrics were computed using first returns with heights greater than 3 m to eliminate ground and under-story returns.

2.3. Shadow-area correction

In order to model tree shade with different topographies and sun angles, the LiDAR-derived CSMs were imported into ESRI’s ArcGrid software (release 9.2) as grid files. Each site’s CSM was placed over a series of artificial planes representing a range of azimuths from 0° to

180° relative to the sun in increments of 15° and slopes from 0° to 54.5° in increments of 10% slope. (ArcGrid measures slope in percent calculated from rise/run.) ArcGrid’s hillshade function was used to artificially illuminate the CSM using the solar illumination angles for four solar zenith angles (SZA) (Table 4). The SZAs were chosen to represent the smallest local solar zenith angle (summer solstice) and the change in solar illumination at 30-day intervals at the Watershed’s location (SZA’s of 29°, 33°, 39°, and 49°). For each slope, azimuth, and SZA, each grid cell of the CSM was marked by ArcGrid’s hillshade function as either illuminated or shadowed by canopy elements within the scene. Fig. 3 shows example output grids. The total number of shadowed cells were summed and divided by the total number of cells to give the proportion of canopy shadowed.

This modeling effectively created a “landscape” of “hills” with slopes ranging from 0° to 54.5° and azimuths ranging from 0° to 180° relative to the sun (183 slope-azimuth combinations). Each of the 80 hills had a single stand type representing one of the permanent plot sites distributed across the combinations of slope and azimuth. This provided 58,560 slope-azimuth-stand-SZA combinations to measure the proportion of sunlit and shadowed area to enable testing of the different topographic corrections: (13 slopes×14 aspects)+(0° slope)×(80 CSMs)=14,640×4 SZAs. The study tools used did not rotate the CSMs, so a single aspect was used for slope=0°.

Gu and Gillespie’s mathematical derivation of the SCS equation provided an intermediate form (Eq. (13)) that could be used to test the accuracy of the SCS term for real forests measured by LiDAR. From the modeling of sunlit and shadowed areas with ArcGrid, this present study had for each of 58,560 slope-aspect-SZA-stand combinations the actual value of the ratio of A/A_n (uncorrected sunlit area to corrected sunlit area). This value could then be compared to the value for the SCS term (Eq. (19)) to test Gu and Gillespie’s assertion that the SCS term estimates A/A_n for complex, real forests. Both the SCS and SCS+C corrections were tested by substituting the A and A_n terms for L and L_n (Eq. (14)), and the C term was computed by substituting $A=L$ in Eq. (7).

3. Results

3.1. Relationship of tree shade to stand characteristics

Tree shade correlates strongly with the rumple index (Fig. 6; Table 5). Correlations of tree shade with the rumple index decreased as the SZA increased but remained high ($R^2=0.94-0.87$ depending on SZA). Tree-shade correlation with stand parameters was higher for parameters that

Table 6
Results of the ASC regression with results for other options investigated for an empirical shadow area topographic compensation solution

ASC: Multiple linear regressions by $\cos(i)$ range with indicator variables				
Independent variable(s)	SZA 29°	SZA 33°	SZA 39°	SZA 49°
ShA $(\cos \alpha \cos \theta)/\cos i$	0.937	0.937	0.888	0.834
Alternatives investigated for ASC regression				
ShA $\cos i$	0.899	0.905	0.864	0.857
ShA $\cos \theta/\cos i$	0.897	0.896	0.850	0.853
Single linear regression for all $\cos(i)$ values with multiple geometric terms selected through backwards stepwise selection. All terms were included.				
ShA $(\cos \alpha \cos \theta)/\cos i, \cos \theta/\cos i, \cos i$	0.876	0.869	0.817	0.810
Single linear regression for all $\cos(i)$ values with single geometric variable				
ShA $\cos i$	0.784	0.761	0.691	0.654
ShA $(\cos \alpha \cos \theta)/\cos i$	0.860	0.742	0.477	0.403
ShA $\cos \theta/\cos i$	0.810	0.702	0.467	0.403
ShA	0.529	0.439	0.309	0.201
Mathematical functions				
SCS+C (Eq. (9))	0.73	0.66	0.51	0.36
SCS (Eq. (10))	0.14	0.11	0.02	0.00

Regression options shown in order of descending compensation accuracy. The ASC regression used the $(\cos \alpha \cos \theta)/\cos i$ variable, and performed multiple regressions by ranges of $\cos(i)$ variable using indicator variables. The ASC regression had the highest performance of all options except for SZA 49°, where an alternative form using the $\cos i$ variable had slightly higher accuracy. Where multiple variable options were investigated for a single approach, the highest R^2 value for each SZA is shown in bold. All regressions and regression variables were significant at $P < 0.001$. Regressions conducted using SPSS release 15.0.

Table 7
ASC regression equations

ASC regression by $\cos(i)$ range	
SZA=29°	
$\cos(i) \geq 0.8$	$ShA_n = 0.204 + 1.183 \times ShA - 0.226 \times SCS$
$\cos(i) 0.5-0.79$	$ShA_n = 0.183 + 0.913 \times ShA - 0.172 \times SCS$
$\cos(i) < 0.3-0.49$	$ShA_n = 0.145 + 0.703 \times ShA - 0.115 \times SCS$
$\cos(i) < 0.3$	$ShA_n = 0.054 + 0.572 \times ShA - 0.052 \times SCS$
SZA=33°	
$\cos(i) \geq 0.8$	$ShA_n = 0.242 + 1.235 \times ShA - 0.278 \times SCS$
$\cos(i) 0.5-0.79$	$ShA_n = 0.211 + 0.952 \times ShA - 0.202 \times SCS$
$\cos(i) < 0.3-0.49$	$ShA_n = 0.159 + 0.771 \times ShA - 0.131 \times SCS$
$\cos(i) < 0.3$	$ShA_n = -0.031 + 0.648 \times ShA - 0.028 \times SCS$
SZA=39°	
$\cos(i) \geq 0.8$	$ShA_n = 0.299 + 1.275 \times ShA - 0.361 \times SCS$
$\cos(i) 0.5-0.79$	$ShA_n = 0.255 + 0.998 \times ShA - 0.253 \times SCS$
$\cos(i) < 0.3-0.49$	$ShA_n = 0.185 + 0.864 \times ShA - 0.165 \times SCS$
$\cos(i) < 0.3$	$ShA_n = -0.091 + 0.611 \times ShA - 0.005 \times SCS$
SZA=49°	
$\cos(i) \geq 0.8$	$ShA_n = 0.133 + 1.143 \times ShA - 0.001 \times SCS$
$\cos(i) 0.5-0.79$	$ShA_n = 0.311 + 1.036 \times ShA - 0.320 \times SCS$
$\cos(i) < 0.3-0.49$	$ShA_n = 0.207 + 0.976 \times ShA - 0.206 \times SCS$
$\cos(i) < 0.3$	$ShA_n = -0.095 + 0.684 \times ShA^a$

All regression coefficients significant ($P < 0.05$) except as noted.

^a SCS correction term for this illumination geometry not significant.

measured tree size (95th percentile height and mean dbh), but lower for other stand parameters (canopy tree count and basal area). Correlation of tree shade with the composite I_{og} index was intermediate. Correlations of tree shade with stand metrics were constant across the range of SZAs (R^2 changes of less than <0.02). Attempts to use combinations of stand parameters in multiple regressions to predict tree shade had similar R^2 values as the individual parameters. The most successful multiple regression had an $R^2=0.73$ and used the standard deviation of LiDAR point heights (“rugosity”) and 95th percentile heights as variables. Canopy tree count and basal area were not significant predictors.

3.2. Topographic tree-shade correction

Two problems were found with the SCS correction. First, the SCS term provides a fixed value for each slope-aspect-SZA combination (Fig. 4). The LiDAR A/A_n ratio, however, differed for every stand. As a general trend, stands with rumple indices <2 had A/A_n curves that were distinct from stands with indices >2 . None of the A/A_n curves, which were derived from real canopy surfaces, matched the SCS curve,

which was predicted for an idealized canopy surface (Gu and Gillespie, 1988). As a result, the SCS correction would fail to give accurate corrections for any of the real canopies used in this study, and the degree of inaccuracy would depend on the canopy characteristics of each stand. The second problem with the SCS correction was that it would over- or under-correct on steep pro- and anti-sun slopes. The combinations of these problems led to inaccurate corrections for shadow area (Table 6).

The SCS+C correction was formulated to mitigate the problems of SCS over correction of radiance for steep slopes (Soenen et al., 2005). The SCS+C correction provided substantially more accurate corrections for all SZAs than did the SCS correction (Table 6). In interpreting the SCS+C results, it is important to keep in mind that the C term was initially proposed as both a way to moderate the over correction inherent in the cosine correction (Eq. (3)) and to model the effects of diffuse sky illumination (Soenen et al., 2005; Teillet et al., 1982). Because our testing does not include the latter factor, the results presented here may not be representative of the performance of the SCS+C correction in real images. The SCS+C correction was also intended to be applied on a per band basis prior to spectral analysis.

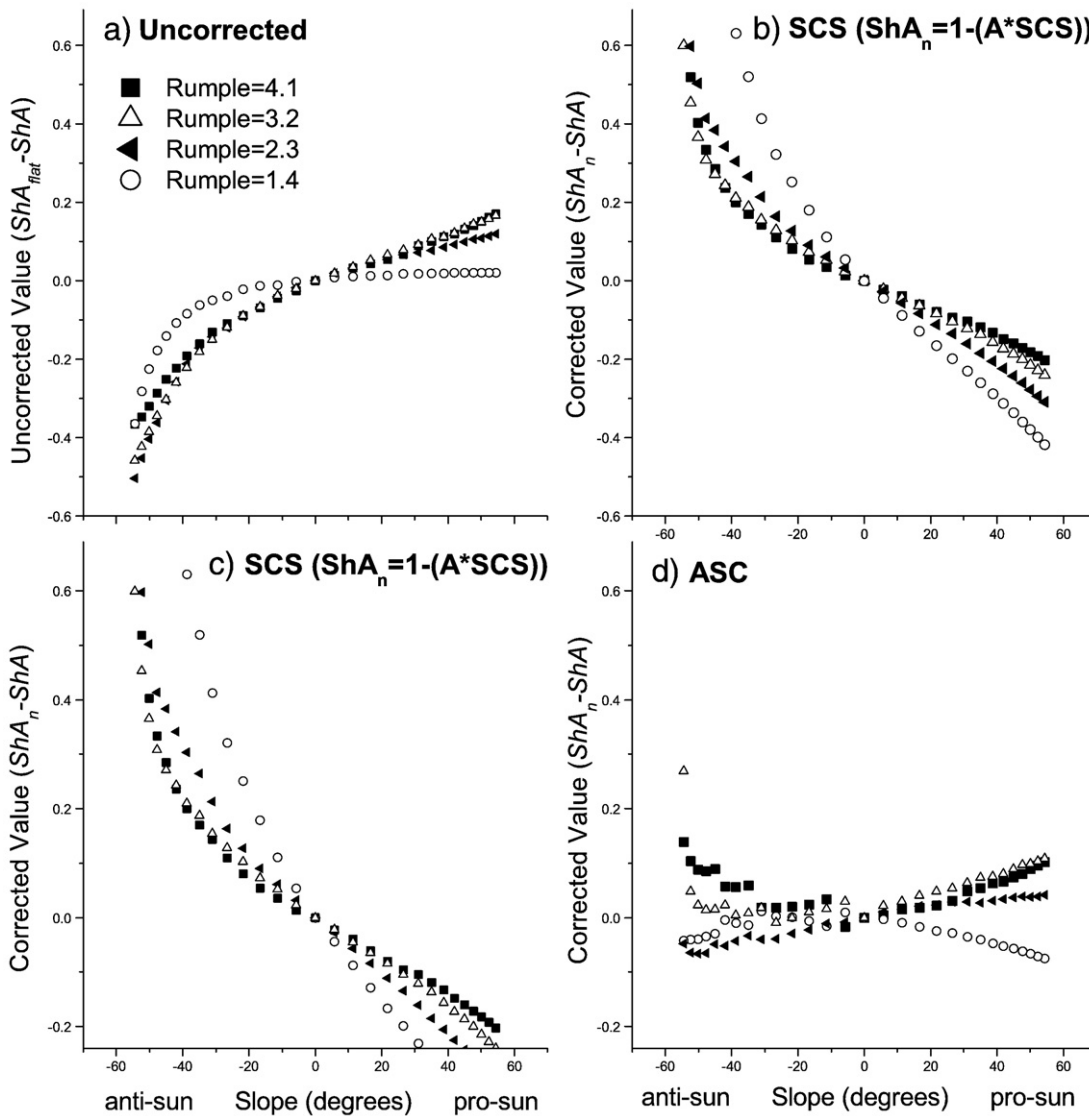


Fig. 7. Correction accuracy for four canopies using the SCS and ASC corrections. Differences between ShA and ShA_{nat} prior to correction also shown for comparison (a). (b) and (c) show the same data plotted against different corrected value ranges to allow comparison with (a) and (d). Results are for $SZA=29^\circ$. Slopes shown are in the principal plane (azimuths 0° and 180° relative to the sun). The 0° slope values are the correct ShA_{nat} values. Breaks in the correction trends in the ASC correction caused by the use of multiple regressions by $\cos(i)$ range.

Applying this correction to shadow area as an estimate of the Shade fraction that would be derived after spectral unmixing, may not be appropriate.

Because the A/A_n curve was unique for each canopy tested, empirical approaches to shadow correction were attempted. A number of different linear regressions were developed and tested for their accuracy in correcting ShA for topographic and SZA change (Table 6). Regressions using any single or combination of geometric variables had an $R^2=0.00$, and regressions using only the shadow area variable (ShA) had poor compensation accuracies. However, including at least one geometric term with the ShA term substantially improved regression results. Regressions that used either the $(\cos\alpha \cos\theta)/\cos i$ or $\cos i$ variable for the geometric term had the highest accuracies.

The most accurate empirical correction was termed the Adaptive Shade Compensation (ASC) algorithm and was based on two independent variables. ASC incorporated the shadow area proportion (ShA) as an estimator of canopy complexity and the inverse of the SCS term (Eq. (19)), $(\cos\alpha \cos\theta)/\cos i$, as an estimator of how the

proportion of shadow area changed based on the geometry of the scene:

$$ShA_n = b_0 + b_1ShA + b_2 \left(\frac{\cos\alpha \cos\theta}{\cos i} \right) \tag{21}$$

(‘Adaptive’ refers to the use of a term that estimates canopy complexity, ShA , and therefore modifies the correction with information about the canopy structure.)

Examination of residuals from the initial ASC regressions suggested that deriving separate regressions for ranges of $\cos(i)$ values would improve accuracy. Indicator variables (Kutner et al., 2004) were used to divide the data set for the regression into four ranges of $\cos(i)$ values based on residual patterns: $\cos(i) \geq 0.8$, 0.5–0.7999, 0.3–0.4999, < 0.3 . A separate regression for each incidence angle range was derived (Table 7). Examination of the significance of the regression coefficients for each subset of the data was used to determine whether the regressions were statistically distinct.

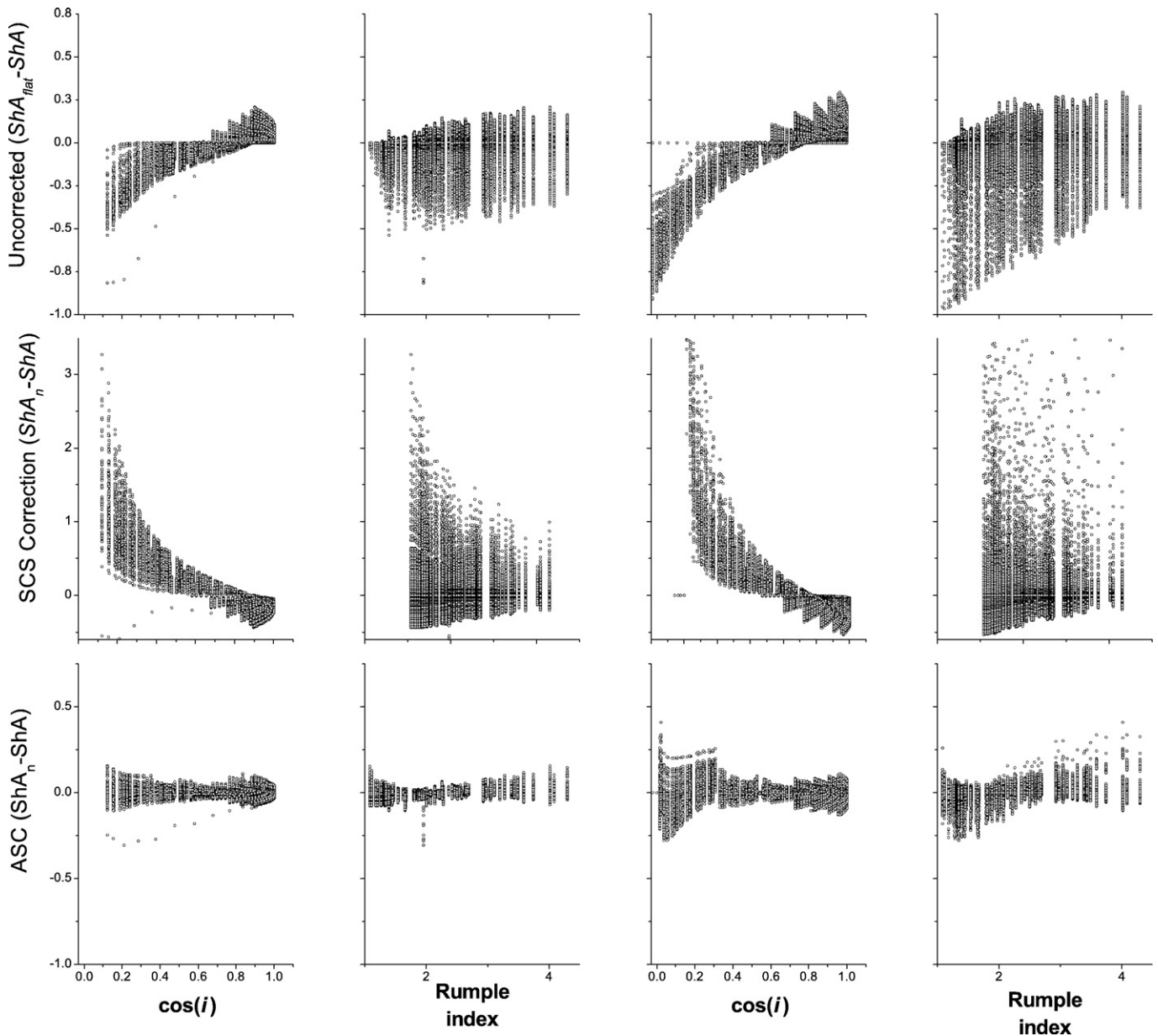


Fig. 8. Correction accuracy for two shadow area compensations for two solar zenith angles (SZAs) with uncorrected values for comparison. Each point is the difference between $ShA_{flat} - ShA$ for uncorrected and $ShA_n - ShA$ for corrected values. Perfect correction would have all points lined up on the zero residual value. Residuals for the SCS correction plotted on a different Y axis than the other two corrections. The ASC regressions produced the most accurate corrections across all $\cos(i)$ values and canopy complexities for both SZA illuminations.

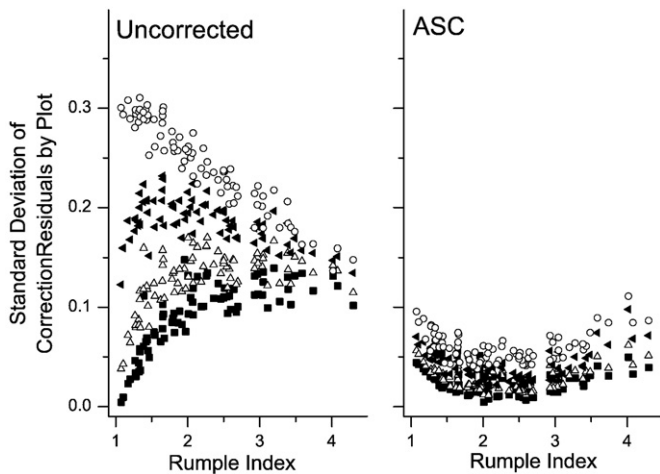


Fig. 9. Accuracy of the ASC topographic compensation method for four solar zenith angles (SZA). Each point is the standard deviation of $Sh_{A_{flat}} - Sh_A$ for uncorrected and $Sh_{A_n} - Sh_A$ values for a single plot and SZA.

Results of the ASC regression are presented at three levels of detail to show different views of the of shadow area correction accuracy as topography and SZA changed: (1) correction residuals ($Sh_{A_{flat}} - Sh_{A_n}$) for a single SZA for slopes on the principal plane (Fig. 7), (2) correction residuals by $\cos(i)$ and canopy complexity for two SZAs (Fig. 8), and (3) standard deviation of correction residuals by canopy complexity for all SZAs (Fig. 9). Residuals are reported to simplify comparison of accuracy between methods and SZAs. As with all correction methods tested, ASC corrections were least accurate for steeper slopes and higher SZAs. However, the multiple regressions by $\cos(i)$ range of the ASC regressions mitigated the under-correction on anti-sun slopes inherent in the SCS correction.

4. Discussion

4.1. Sources of spectral shade in forest scenes

A large body of work has focused on understanding the reflectance behavior of forests (e.g., Franklin et al., 1991; Li et al., 1995; Verhoef, 1984). Less work has been devoted to understanding the relationship between canopies and Shade. Self-shadowing caused by canopy roughness (along with the geometry of the incidence and exitance angles) has a major effect on the reflectance observed by a sensor (Dymond et al., 2001). In addition to tree and topographic shade, three other sources of shade contribute to the observed shade in forest scenes (Gillespie et al., 2006):

- Small-scale shadowing from fine structures of a tree such as leaves, needles, and small branches (leaf shade)
- Changes in incidence angle across the surfaces of the individual elements of the tree (geometric shade)
- Absorption of light by the tree's surfaces

Gillespie et al. (2006) found that these factors vary with tree morphology, stand structural stage, species, and possibly tree age in a mixed forest in Maryland, USA. Tree shade had twice the mean contribution to SMA Shade as leaf shade. Gillespie et al. (2006) found that more work is needed to understand the contributions of geometric shade and absorption. Topographic shade was not a factor because their study site was flat.

The high values for tree shade for many stands in flat terrain in this study is in line with Gillespie et al.'s (2006) finding that tree shade is the dominant contributor to Shade in forest scenes. However, the methods of our study probably overstate the contribution of tree shade to the actual Shade fraction in a scene. The CSMs created using the Fusion software represents trees as solid, opaque shapes. Real conifer

trees have unresolved gaps between branches that permit some light to brighten the tree shade. Similarly, ArcGrid models only light coming from the modeled sun position. It cannot model diffuse skylight or light reflected off of nearby canopies or hills. All these sources will brighten the tree shade in the spectra of a real forest canopy. On the other hand, other sources of canopy Shade such as leaf shade will serve to add Shade to each pixel. The shadow area corrections done with ASC will be more accurate if the tree-shade models prepared with LiDAR data are first calibrated against measured Shade fractions in an image.

4.2. Interpretation of tree shade

The Shade fraction of an image has been used in a number of forest studies as a measure of either canopy roughness or canopy structure. This study supports this interpretation. Our goal in pursuing this line of inquiry had been that modeling tree shade from canopy LiDAR datasets would allow better estimation of traditional stand measurements such as tree size, basal area, and density that have proven difficult to derive from moderate-resolution scanners such as Landsat. Our results do not support this expectation. For example, the moderate correlation between tree shade and stand height ($R^2=0.60$), was unexpected (Fig. 6).

The low correlations between tree shade and traditional stand measurements are in line with those from a study that compared results from multiple remote-sensing methods for Pacific Northwest forests (Lefsky et al., 2001). That study compared a Tasseled Cap transformation of a Landsat TM image and a principle components analysis of an Airborne Visible/Infrared Imaging Spectrometer (AVIRIS) image (25-m resolution). Lefsky et al.'s results combined with those from this study suggests a fundamental limitation to the ability to estimate many of the stand measurements that have traditionally been used by forest managers and ecologists using data from medium resolution optical instruments alone.

Forests are heterogeneous and have ranges of combinations of structural characteristics. Forest ecologists have not been able to develop a single metric that captures this complexity and typically describe structure as the combination of traits (e.g., mean dbh, standard deviation dbh, and tree count). It is not surprising that a single measure of stand structure, the rumple index and its associated tree shade, cannot capture that complexity.

For example, the correlation of tree shade with tree size in this study was moderate (Table 5). The common view is that tree size is associated with the development of stand complexity (Oliver and Larson, 1996), which in turn creates canopy complexity and higher tree shade. Our data show that while short stands have less tree shade, taller stands can have a wide range of tree shade. This supports the observation that stands follow a large number of developmental pathways. Large trees are necessary to create higher ranges of stand complexity but are not a direct correlate. Variation in size, spatial arrangement, and the number of trees all influence the canopy complexity made possible by the stand height. The moderate correlation of tree shade with plot characteristics is in line with the correlation of different plot measurements. In the plots used in this study, for example, mean dbh and 95th percentile height have an $R^2=0.67$ (Table 5). This is similar to the correlation between the rumple index and mean dbh ($R^2=0.65$) or 95th percentile height ($R^2=0.60$).

Canopy complexity appears to be an emergent property of the unique combination of processes – stand establishment, competitive exclusion, disturbance, and human management – that shape each stand. A major source of ambiguity in interpreting tree shade is that the relationship between the stand structure – the size and arrangement of trees – and canopy complexity – the geometric shape of the canopy surface – is poorly understood. Fully exploring this relationship requires spatially explicit maps of stand trees and the surface of the canopy. Studying patterns of canopy complexity through tree shade allows canopy complexity to be studied across large areas.

A growing body of work has started to explore the relationship between canopy complexity and stand development (Bradshaw and Spies, 1992; Franklin and Van Pelt, 2004; Ishii and McDowell, 2002; Larson and Franklin, 2006; Van Pelt and Nadkarni, 2004; Winter et al., 2002b). Disturbance or management history can be deduced from differences in the geometric canopy complexity (Zenner, 2004, 2005; Zenner and Hibbs, 2000). The habitat value of young, second-growth stands varies with stand and canopy structural complexity (Aubry et al., 1997; FEMAT, 1993; McKenzie et al., 2000; Parker et al., 2002). Knowing that tree shade correlates with an emergent ecological value creates a new way to study forests.

4.3. Topographic shade correction

Gu and Gillespie (1988) had no way to measure the sunlit area of the canopy directly to determine how accurately the radiance SCS correction (Eq. (8)) estimated the actual sunlit area. Instead, they and Soenen et al. (2005) used modeled canopies and modeled radiance with a single SZA each to measure how accurately the SCS equation estimated the relationship between canopy structure and changes in sunlit/shadowed area with topography. Both of those studies reported accurate corrections by the SCS equation for low to moderate slopes, indicating that the SCS equation worked well for idealized canopies.

The SCS correction was developed using modeled tree stands with heights of 15 m and tested on a scene with trees of similar size (Gu and Gillespie, 1988). The work reported here examined a more complete range of tree heights; just 15 of the 80 plots used in this study have 95th percentile heights below 20 m. In the comparatively simple stands modeled by Gu and Gillespie (1988) and Soenen et al. (2005), the SCS term correlated well with changes in sunlit area. This correlation appears to break down for more complex canopies, at least as assessed by LiDAR data in which canopies are modeled as solid shapes without the small gaps that characterize real ones. The unexpectedly poor correlation of the SCS term (Eq. (19)) with the A/A_n ratio can be seen in the inaccurate SCS correction results even at low and moderate slopes (Fig. 7). This source of inaccuracy, however, was overwhelmed by the SCS equation's over- and under-correction on steep pro- and anti-sun slopes (Figs. 8 and 9).

The empirical ASC regressions, on the other hand, showed comparatively little variation in correction accuracy with changes in canopy complexity or for steep pro- and anti-sun slopes (Figs. 7–9). Like the C (Eq. (6)) and SCS+C (Eq. (9)) corrections, the ASC regressions combined a geometric term (the inverse of the SCS term, Eq. (19)) and an empirical term (shadow area, ShA , as an estimate of the tree-shade component of the SMA shade fraction). Unlike the C and SCS+C equations, however, the ASC regressions have coefficients that allowed the interaction of the SCS and ShA terms to vary. This models real canopies where the shadow area for a given slope-aspect-SZA combination varies with canopy complexity. In doing so, the ASC regressions met the requirements set out by Schaaf et al. (1994) that a full understanding of the bidirectional reflectance distribution function for forests requires knowledge of both the geometry of the image and the structure of the forest canopy.

The ASC method should be robust across a variety of conifer forest systems. However, the ASC regression coefficients computed for this study are specific to the given SZA's and closed-canopy conifer forests. In order to facilitate the use of the ASC technique for other studies, the CSMs and computer tools for modeling tree shade and topographic shade are available from the corresponding author. For studies of forests with canopies that are substantially different than those in the Pacific Northwest, the tools can be used with the CSMs created from LiDAR data of those forest types.

5. Conclusion

This study used LiDAR data to model changes in a dominant contributor to Shade in canopies, tree shade produced by canopy self-

shadowing, in Pacific Northwest forests. Tree shade correlates well with the geometrical complexity of canopies, but less well to common stand measurements such as tree height, diameter, and count. Tree shade is an emergent property that results from tree size, variations in heights within canopies, and tree spacing. Because many combinations of these variables can produce the same tree shade, it is difficult to estimate the relative contribution of each factor. As a result, remote sensing that uses the Shade to estimate stand structure will be limited in its ability to provide information on plot characteristics that have been traditionally used for stand management and ecological studies. The results in this paper, however, support interpretation of Shade as a function of canopy complexity, which is an important ecological characteristic in its own right.

The use of tree shade to measure canopy complexity has been limited by the strong effect of topography on tree shade. Several approaches have been proposed to improve topographic radiance correction of forest scenes, including the Sun-Canopy-Sensor (SCS) algorithm. Because SCS corrects radiance by correcting the area of sunlit canopy, it can also be used to correct its complement, the area of shadowed canopy. SCS has limitations that prevent accurate correction of topographic tree shade across a full range of incidence angles and canopy complexities. This study developed a new approach, the Adaptive Shade Compensation (ASC) algorithm that combines the geometric approach of SCS with an empirical term that uses the measured Shade proportion as an independent variable. This allows the regression to compensate for the change in self-shadowing behavior as canopies become more complex. The ASC approach provides more accurate topographic correction of tree shade across the range of tested solar illumination angles, incidence angles, and canopy complexities.

Acknowledgements

NASA (Earth and Space Science Fellowship Program grant NNX07AN75H and grant NNG04HZ55C), the Watersheds Services Division of Seattle Public Utilities, and the King County government of Washington state provided funding support. The Watersheds Services Division of Seattle Public Utilities shared their permanent plot data and the raw LiDAR data set that was originally acquired by King County. Comments by James Freund, Andrew J. Larson, and Linda Winters improved earlier drafts of this article. We thank the four anonymous reviewers for their suggestions.

References

- Acker, S. A., Sabin, T. E., Ganio, L. M., & McKee, W. A. (1998). Development of old-growth structure and timber volume growth trends in maturing Douglas-fir stands. *Forest Ecology and Management*, 104, 265–280.
- Adams, J. B., & Gillespie, A. R. (2006). *Remote sensing of landscapes with spectral images: A physical modeling approach*. New York: Columbia University Press.
- Adams, J. B., Sabol, D. E., Kapos, V., Filho, R. A., Roberts, D. A., Smith, M. O., et al. (1995). Classification of multispectral images based on fraction endmembers: Application to land-cover change in Brazilian Amazon. *Remote Sensing of the Environment*, 52, 137–154.
- Adams, J. B., Smith, M. O., & Gillespie, A. R. (1993). Imaging spectroscopy: Interpretation based on spectral mixture analysis. In C. M. Pieters & P. Englert (Eds.), *Remote geochemical analysis: Elemental and mineralogical composition*, Vol. 7 (pp. 145–166). NY: Cambridge Univ. Press.
- Aubry, K. B., West, S. D., Manuwal, D. A., Stinger, A. B., Erickson, J. L., & Pearson, S. (Eds.). (1997). *Wildlife use of managed forests: A landscape perspective volume 2: West-side Studies Research Results. Technical Report TFW-WL4-98-002*. Olympia, WA: Washington State Department of Timber, Fish, and Wildlife.
- Bradshaw, G. A., & Spies, T. A. (1992). Characterizing canopy gap structure in forests using wavelet analysis. *Journal of Ecology*, 80, 205–215.
- Cohen, W. B., & Spies, T. A. (1992). Estimating structural attributes of Douglas-fir/western hemlock forest stands from Landsat and SPOT imagery. *Remote Sensing of the Environment*, 41, 1–17.
- Dymond, J., Shepherd, J. D., & Qi, J. (2001). A simple physical model of vegetation canopy reflectance. *Remote Sensing of Environment*, 75, 350–359.
- Erckmann, J., Chinn, A., Flagor, S., Kurko, K., Freeman, J., Little, R., et al. (2000). Final cedar river watershed habitat conservation plan. (pp. 3.2-1 to 3.2-14). City of Seattle, Seattle, WA, USA.

- Foody, G. M. (2004). Sub-pixel methods in remote sensing. In S. M. DeJong & F. D. van der Meer (Eds.), *Remote sensing image analysis: Including the spatial domain* (pp. 37–50). Boston, MA: Kluwer Academic Publishers.
- Forest Ecosystem Management Assessment Team (FEMAT) (1993). *Forest ecosystem management: An ecological, economic, and social assessment — Report of the Forest Ecosystem Management Assessment Team*. Portland, Oregon, USA: USDA, USDI, U.S. Department of Commerce, and Environmental Protection Agency.
- Franklin, J., Davis, F. W., & Lefebvre, P. (1991). Thematic Mapper analysis of tree cover in semiarid woodlands using a model of canopy shadowing. *Remote Sensing of Environment*, 36, 189–202.
- Franklin, J. F., & Dyrness, C. T. (1988). *Natural vegetation of Oregon and Washington*. Corvallis, OR: Oregon State University Press.
- Franklin, J. F., & Van Pelt, R. (2004). Spatial aspects of structural complexity in old-growth forests. *Journal of Forestry*, 102, 22–27.
- Franklin, J. F., Spies, T. A., Van Pelt, R., Carey, A. B., Thornburgh, D. A., et al. (2002). Disturbances and structural development of natural forest ecosystems with silvicultural implications, using Douglas-fir forests as an example. *Forest Ecology and Management*, 155, 399–423.
- Gillespie, A. R., Gilson, L., Gillespie, M. A., & Kane, V. R. (2006). A framework for estimating unresolved spectral shade. In J. A. Sobrino (Ed.), *Second recent advances in quantitative remote sensing* (pp. 385–390). Spain: Publicacions de la Universitat de València.
- Greenberg, J. A., Dobrowski, S. Z., & Ustin, S. L. (2005). Shadow allometry: Estimating tree structural parameters using hyperspatial image analysis. *Remote Sensing of Environment*, 97, 15–25.
- Gu, D., & Gillespie, A. (1988). Topographic normalization of Landsat TM images of forest based on subpixel sun-canopy-sensor geometry. *Remote Sensing of Environment*, 64, 166–175.
- Ishii, H., & McDowell, N. (2002). Age-related development of crown structure in coastal Douglas-fir trees. *Forest Ecology and Management*, 169, 257–270.
- Kutner, M. H., Nachtsheim, C. J., & Neter, J. (2004). *Applied linear regression models* (pp. 314–321). New York, NY: McGraw-Hill/Irwin.
- Larson, J. A., & Franklin, J. F. (2006). Structural segregation and scales of spatial dependency in *Abies amabilis* forests. *Journal of Vegetation Science*, 17, 489–498.
- Leboeuf, A., Beaudoin, A., Fournier, R. A., Guindon, L., Luther, J. E., & Lambert, M. -C. (2007). A shadow fraction method for mapping biomass of northern black spruce forests using QuickBird imagery. *Remote Sensing of Environment*, 110, 488–500.
- Lefsky, M. A., Cohen, W. B., & Spies, T. A. (2001). An evaluation of alternative remote sensing products for forest inventory, monitoring, and mapping of Douglas-fir forests in western Oregon. *Canadian Journal of Forest Research*, 31, 78–87.
- Li, X., & Strahler, A. H. (1985). Geometric-Optical Modeling of a Conifer Forest Canopy. *IEEE Transactions on Geoscience and Remote Sensing*, GE-23, 705–721.
- Li, X., Strahler, A. H., & Woodcock, C. E. (1995). A hybrid geometric optical radiative transfer approach for modeling albedo and directional reflectance of discontinuous canopies. *IEEE Transactions on Geoscience and Remote Sensing*, 33, 466–480.
- Lu, D., Moran, E., & Batistella, M. (2003). Linear mixture model applied to Amazonian vegetation classification. *Remote Sensing of Environment*, 87, 456–469.
- Lutz, J. A., & Halpern, C. B. (2006). Tree mortality during early forest development: A long-term study of rates, causes, and consequences. *Ecological Monographs*, 76, 257–275.
- McGaughey, R. J., & Carson, W. W. (2003). Fusing LIDAR data, photographs, and other data using 2D and 3D visualization techniques. *Proceedings of terrain data: Applications and visualization — Making the connection, October 28–30, 2003* (pp. 16–24). Charleston, South Carolina: American Society for Photogrammetry and Remote Sensing.
- McGaughey, R. J., Carson, W. W., Reutebuch, S. E., & Andersen, H. -E. (2004). Direct measurement of individual tree characteristics from LIDAR data. *Proceedings of the 2004 Annual ASPRS Conference, May 23–28 2004*. Denver, Colorado: American Society of Photogrammetry and Remote Sensing Unpaginated CD-ROM.
- McKenzie, D., Halpern, C. B., & Nelson, C. R. (2000). Overstory influences on herb and shrub communities in mature forests of western Washington, U.S.A. *Canadian Journal of Forest Research*, 30, 1655–1666.
- Minnaert, N. (1941). The reciprocity principle in lunar photometry. *Astrophysics Journal*, 93, 403–410.
- Ogunjemiyo, S., Parker, G., & Roberts, D. (2005). Reflections in bumpy terrain: Implications of canopy surface variations for the radiation balance of vegetation. *IEEE Geoscience and Remote Sensing Letters*, 2, 90–93.
- Oliver, C. D., & Larson, B. C. (1996). *Forest stand dynamics, updated edition*. New York: John Wiley and Sons.
- Parker, G. G., Davis, M. M., & Chapotin, S. M. (2002). Canopy light transmittance in Douglas-fir-western hemlock stands. *Tree Physiology*, 22, 147–157.
- Parker, G. G., Harmon, M. E., Lefsky, M. A., Chen, J., Van Pelt, R., Weis, S. B., Thomas, S. C., Winner, W. E., Shaw, D. C., & Franklin, J. F. (2004). Three-dimensional structure of an old growth Pseudotsuga-Tsuga canopy and its implications for radiation balance, microclimate, and gas exchange. *Ecosystems*, 7, 440–453.
- Peddle, D. R., Hall, F. G., & LeDrew, E. F. (1999). Spectral mixture analysis and geometric-optical reflectance modeling of boreal forest biophysical structure. *Remote Sensing of Environment*, 67, 288–297.
- Poage, N. J., & Tappeiner, J. C., II (2005). Tree species and size structure of old-growth Douglas-fir forests in central western Oregon, USA. *Forest Ecology and Management*, 204, 329–343.
- Roberts, D. A., Ustin, S. L., Ogunjemiyo, S., Greenberg, J., Dobrowski, S. Z., Chen, J., & Hinkley, T. M. (2004). Spectral and structural measures of northwest forest vegetation at leaf to landscape scales. *Ecosystems*, 7, 545–562.
- Sabol Jr., D. E., Gillespie, A. R., Adams, J. B., Smith, M. O., & Tucker, C. J. (2002). Structural stage in Pacific Northwest forests estimated using simple mixing models of multi-spectral images. *Remote Sensing of Environment*, 80, 1–16.
- Schaaf, C. B., Li, X. W., & Strahler, A. H. (1994). Topographic effects on bidirectional and hemispherical reflectances calculated with a geometric-optical canopy model. *IEEE Transactions on Geoscience and Remote Sensing*, 32, 1186–1193.
- Settle, J. J., & Drake, N. (1993). Linear mixing and the estimation of ground cover proportions. *International Journal of Remote Sensing*, 14, 1159–1177.
- Smith, D. M., Larson, B. C., Kelty, M. J., & Ashton, P. M. S. (1997). *The practice of silviculture: Applied forest ecology*. New York: John Wiley & Sons, Inc.
- Soenen, S. A., Peddle, D. R., & Coburn, C. A. (2005). SCS+C: A modified sun-canopy-sensor topographic correction in forested terrain. *IEEE Transactions on Geoscience and Remote Sensing*, 43, 2148–2159.
- Soenen, S. A., Peddle, D. R., Coburn, C. A., Hall, R. J., & Hall, F. G. (2008). Improved topographic correction of forest image data using a 3-D canopy reflectance model in multiple forward mode. *International Journal of Remote Sensing*, 29, 1007–1027.
- Song, C. H., & Woodcock, C. E. (2002). The spectral/temporal manifestation of forest succession in optical imagery — The potential of multitemporal imagery. *Remote Sensing of Environment*, 82, 285–302.
- Spies, T. A., & Franklin, J. F. (1991). The structure of natural young, mature, and old-growth Douglas-fir forests in Oregon and Washington. In L. F. Ruggiero, K. B. Aubry, A. B. Carey, & M. H. Huff (Eds.), *Wildlife and Vegetation of Unmanaged Douglas-fir Forests. General Technical Report PNW-GTR-285* (pp. 91–110). Portland, OR: U.S. Dept. of Agriculture, Forest Service, Pacific Northwest Research Station.
- Teillet, P. M., Guindon, B., & Goodenough, D. G. (1982). On the slope-aspect correction of multispectral scanner data. *Canadian Journal of Remote Sensing*, 8, 84–106.
- Tottrup, C., Rasmussen, M. S., Samek, J., & Skole, D. L. (2007). Towards a generic approach for characterizing and mapping tropical secondary forests in the highlands of mainland Southeast Asia. *International Journal of Remote Sensing*, 6, 1263–1284.
- USDA Forest Service. (2007). FUSION software, version 2.51. Pacific Northwest Research Station. <http://forsys.cfr.washington.edu/fusion.html>. Last accessed May 31, 2007.
- Van Pelt, R., & Nadkarni, N. M. (2004). Development of canopy structure in Pseudotsuga menziesii forests in the southern Washington Cascades. *Forest Science*, 50, 326–341.
- Verhoef, W. (1984). Light scattering by leaf layers with application to canopy reflectance modeling: The SAIL method. *Remote Sensing of Environment*, 16, 125–141.
- Vincini, M., & Frazzi, E. (2003). Multitemporal evaluation and topographic normalization methods on deciduous forest TM data. *IEEE Transactions on Geoscience and Remote Sensing*, 41, 2586–2590.
- Waring, R. H., & Franklin, J. F. (1979). Evergreen coniferous forests of the Pacific Northwest. *Science*, 204, 1380–1386.
- Winter, L. E., Brubaker, L. B., Franklin, J. F., Miller, E. A., & DeWitt, D. Q. (2002). Initiation of an old-growth Douglas-fir stand in the Pacific Northwest: a reconstruction from tree-ring records. *Canadian Journal of Forest Research*, 32, 1039–1056.
- Winter, L. E., Brubaker, L. B., Franklin, J. F., Miller, E. A., & DeWitt, D. Q. (2002). Canopy disturbances over the five-century lifetime of an old-growth Douglas-fir stand in the Pacific Northwest. *Canadian Journal of Forest Research*, 32, 1057–1070.
- Zenner, E. K. (2004). Does old-growth condition imply high live-tree structural complexity? *Forest Ecology and Management*, 195, 243–258.
- Zenner, E. K. (2005). Investigating scale-dependent stand heterogeneity with structure-area-curves. *Forest Ecology and Management*, 209, 87–100.
- Zenner, E. K., & Hibbs, D. E. (2000). A new method for modeling the heterogeneity of forest structure. *Forest Ecology and Management*, 129, 75–87.